Organic & Biomolecular Chemistry

Cite this: *Org. Biomol. Chem.*, 2011, **9**, 3331

www.rsc.org/obc

PAPER

Intramolecular homolytic substitution of sulfinates and sulfinamides – a computational study†‡

Sara H. Kyne,*§[a,b] Heather M. Aitken,[a,b] Carl H. Schiesser,[a,b] Emmanuel Lacôte,¶[c] Max Malacria,[c] Cyril Ollivier[c] and Louis Fensterbank*[c]

Received 8th January 2011, Accepted 21st February 2011
DOI: 10.1039/c1ob05043e

Ab initio and density functional theory (DFT) calculations predict that intramolecular homolytic substitution by alkyl radicals at the sulfur atom in sulfinates proceeds through a smooth transition state in which the attacking and leaving radicals adopt a near collinear arrangement. When forming a five-membered ring and the leaving radical is methyl, G3(MP2)-RAD//ROBHandHLYP/6-311++G(d,p) calculations predict that this reaction proceeds with an activation energy ($\Delta E_1^{\ddagger}$) of 43.2 kJ mol^{-1}. ROBHandHLYP/6-311++G(d,p) calculations suggest that the formation of five-membered rings through intramolecular homolytic substitution by aryl radicals at the sulfur atom in sulfinates and sulfinamides, with expulsion of phenyl radicals, proceeds with the involvement of hypervalent intermediates. These intermediates further dissociate to the observed products, with overall energy barriers of 45–68 kJ mol^{-1}, depending on the system of interest. In each case, homolytic addition to the phenyl group competes with substitution, with calculated barriers of 51–78 kJ mol^{-1}. This computational study complements and provides insight into previous experimental observations.

Introduction

Free radical homolytic substitution chemistry offers the synthetic practitioner the ability to efficiently construct higher heterocycles under conditions that are often milder than those of the corresponding ionic chemistry.[1,2] The majority of reported examples involve intramolecular attack at divalent chalcogen to afford the corresponding sulfur,[3–10] selenium[11–16] or tellurium[17] containing ring. The examples shown in Scheme 1 illustrate the richness of this chemistry; several radical types as well as tandem (cascade) processes bear witness to the maturity that this chemistry has achieved in recent years.[18–20]

Less common has been the use of homolytic substitution chemistry at oxidized chalcogens. Beckwith and Boate reported over twenty years ago that these reactions at sulfoxides proceed with inversion of configuration.[21] This observation necessitates the involvement of a backside attack transition state, such as **1** and similar to that involved in S_N2 chemistry, or a hypervalent intermediate, such as **2**, that is too short-lived to undergo pseudorotation prior to dissociation (Scheme 2).[21] We are unaware of homolytic substitution chemistry having been carried out on oxidized selenium or tellurium.

Recently, some of us have been exploring homolytic substitution at oxidized sulfur functionalities.[22] To that end, we recently reported a study of intramolecular free radical reactions at sulfinates and sulfinamides with the aim of providing insight into: (1) the nature of the radical leaving group; (2) the tethering atom; (3) the size of the ring being created and (4) the stereochemistry of the chemistry in question.[22] This study showed that these reactions involving sulfinates and sulfinamides are efficient, and can proceed even with an unfavourable aryl leaving group. For example, when sulfinate **3** (Y = O) was treated with tributyltin hydride (slow addition) under standard radical conditions, sultine **4** (Y = O) was isolated in 62% yield along with quantities of the biaryl compound **5** (Scheme 3).[22] Not unexpectedly, when the *p*-tolyl leaving group was replaced with *tert*-butyl, **4** was isolated in near quantitative yield. Similar results were obtained with the sulfinamide **3** (Y = NH), while the *N*-methylsulfinamide **3** (Y = NMe) afforded **4** in considerably lower yield.[22] The key questions that these results pose are: why do these reactions work

[a]*School of Chemistry, Bio21 Molecular Science and Biotechnology Institute, The University of Melbourne, Victoria, 3010, Australia*
[b]*ARC Centre of Excellence for Free Radical Chemistry and Biotechnology, Australia*
[c]*UMPC Université Paris 06, Institut Parisien de Chimie Moléculaire, 4 place Jussieu, C. 229, 75005, Paris, France. E-mail: louis.fensterbank@upmc.fr; Tel: +33 144 27 73 60*

† In memory of Athel Beckwith who inspired and catalysed free radical research in Australia and beyond.

‡ Electronic supplementary information (ESI) available: Scheme S1, Fig. S1 and S2, optimized geometries and energies for all structures in this study (Gaussian Archive Entries). See DOI: 10.1039/c1ob05043e

§ Current address: WestCHEM Department of Pure and Applied Chemistry, University of Strathclyde, Glasgow, UK G1 1XL. Email: sara.kyne@strath.ac.uk; Tel: +44 141 548 2296.

¶ Current address: Institut de Chimie des Substances Naturelles CNRS, Avenue de la Terrasse, 91198 Gif-sur-Yvette Cedex, France.

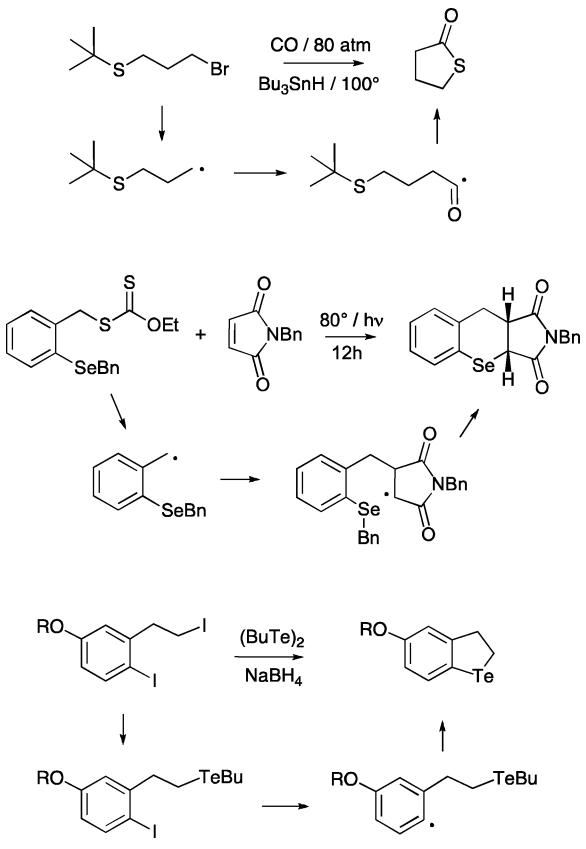

Scheme 1

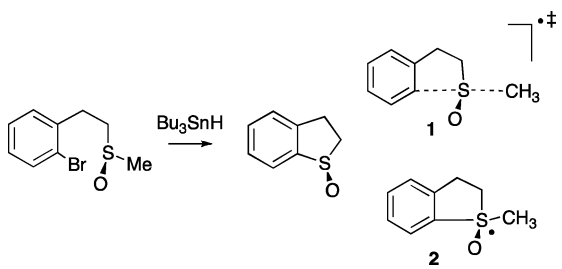

Scheme 2

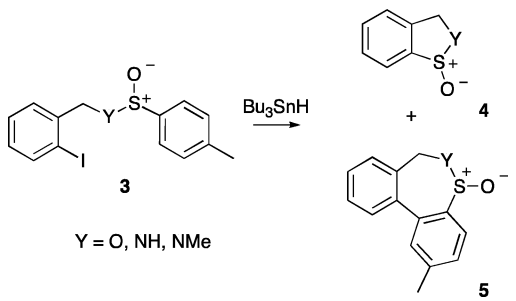

Scheme 3

with an (unfavourable) aryl leaving radical, and how does the methyl substitution affect these reactions?

In order to answer these questions, and to provide further insight into homolytic substitution chemistry involving sulfinates and sulfinamides, we sought recourse to computational chemistry. We now report the results of *ab initio* and density functional calculations involving intramolecular radical attack at these sulfur-containing functional groups.

Computational methods

Ab initio and density functional theory (DFT) calculations were carried using the Gaussian 03 and 09 programs.[23] Geometry optimizations were performed with standard gradient techniques at HF, MP2 and BHandHLYP levels of theory, using restricted methods for closed-shell systems.[24] Many DFT methods, including B3LYP, perform poorly for radical systems, and this is often associated with an inadequate treatment of exchange terms.[24] Zipse showed some time ago that, as a DFT method, BHandHLYP provides a good compromise,[25] and we reported that this method often provides data that reflect those obtained using higher correlation methods such as QCISD or CCSD(T).[25–27]

All ground and transition states in this study were verified by vibrational frequency analysis. Spin contamination proved to be a significant problem for some open-shell systems, especially for transition states and hypervalent intermediates, with UHF, UMP2 and UBHandHLYP methods providing values of $\langle s^2 \rangle$ often in excess of 2 before annihilation of quartet contamination. QCISD and CCSD(T) were much better behaved, with $\langle s^2 \rangle$ mostly below 0.87. As a result, all optimizations of open-shell molecules at these levels were carried out using restricted open shell methods (ROHF, ROBHandHLYP). Standard basis sets available in Gaussian 03 and 09 were used. Further single-point ROMP2, QCISD, CCSD(T) and G3(MP2)-RAD calculations were performed on selected ROBHandHLYP/6-311++G(d,p) optimized structures as detailed in Table 1. Zero-point vibrational energy (ZPE) corrections have been applied to all optimized structures.

Optimized geometries and energies for all structures in this study (Gaussian Archive entries) are available as ESI.‡

Results and discussion

Benchmarking

In order to instill confidence in the computational methods employed, we began this study by benchmarking various levels of theory for the "parent" reaction depicted in Scheme 4; this would provide an understanding of any computational limitations. Searching of the $C_4H_9O_2S$ potential energy surface located structures **6** and **7** as well as the product sultine and methyl radical; **7** proved to correspond to a transition state by vibrational frequency analysis. Structure **7** is displayed in Fig. 1,‡ while key features at each optimized level of theory are listed in Table 1, together with calculated energy data ($\Delta E_1^{\ddagger}$, $\Delta E_2^{\ddagger}$, Scheme 4).

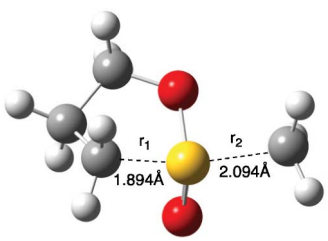

Fig. 1 ROBHandHLYP/6-311++G(d,p) optimised structure of transition state **7**. Data at other levels of theory are listed in Table 1.

Table 1 Calculated activation energies ($\Delta E_1^{\ddagger}$, $\Delta E_2^{\ddagger}$) for the cyclization of radical **6** (Scheme 4), and key data for transition structure **7**

Level of theory	$\Delta E_1^{\ddagger a}$	$\Delta E_1^{\ddagger}$ + ZPE^a	$\Delta E_2^{\ddagger a}$	$\Delta E_2^{\ddagger}$ + ZPE^a	$r_1{}^b$	$r_2{}^b$	$\nu_{TS}{}^c$
ROHF/6-31G(d)	142.0	149.3	136.7	154.6	1.876	2.014	513i
ROHF/6-311G(d,p)	145.3	151.8	140.3	157.3	1.882	2.010	490i
ROBHandHLYP/6-311G(d,p)	77.9	83.8	60.1	73.7	1.894	2.087	375i
ROBHandHLYP/6-311++G(d,p)	81.9	87.8	62.4	75.9	1.894	2.094	385i
ROMP2/6-311++G(d,p)//ROBHandHLYP/6-311++G(d,p)	51.9		38.1				
QCISD/6-311++G(d,p)//ROBHandHLYP/6-311++G(d,p)	72.0		54.7				
QCISD/aug-cc-pVDZ//ROBHandHLYP/6-311++G(d,p)	54.8		34.8				
CCSD(T)/6-311++G(d,p)//ROBHandHLYP/6-311++G(d,p)	61.9		45.7				
CCSD(T)/aug-cc-pVDZ//ROBHandHLYP/6-311++G(d,p)	43.1		23.7				
G3(MP2)-RAD//ROBHandHLYP/6-311++G(d,p)	43.2		24.4				

^{a} Energies in kJ mol^{-1}. ^{b} Key transition structure separations in Å (see Fig. 1). ^{c} Transition state vector (imaginary) frequency (cm^{-1}).

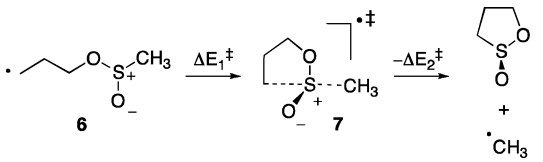

Scheme 4

Inspection of Fig. 1 reveals that transition state **7** is "late" in the direction of reaction depicted in Scheme 4, with the attacking separation (r_1) significantly shorter than the leaving distance (r_2); at the ROBHandHLYP/6-311++G(d,p) level of theory, these separations were calculated to be 1.894 and 2.094 Å, respectively. This is not surprising given that the methyl radical is a poor leaving group in comparison with the incoming primary radical.

These data are to be compared with those from previous calculations; MP2/6-31G(d,p) calculations predict a (symmetrical) transition state distance of 1.927 Å during the attack of methyl radical at the sulfur atom in methylsulfoxide,[30] while distances of about 1.9 Å are calculated for the transition structures involved in alkyl radical cyclisations in sulfides.[31]

The "lateness" of transition state **7** is also reflected in the energy data provided in Table 1; the cyclization of **6** is calculated to be endothermic at all levels of theory used in this study. Table 1 clearly shows that electron correlation is important in these calculations as ROHF methods predict barriers for both the forward and reverse reaction to be over 100 kJ mol^{-1} higher that those calculated at the most reliable method, namely G3(MP2)-RAD. The data also show that the effects of correlation have mostly converged to the G3(MP2)-RAD value using CCSD(T)/aug-cc-pVDZ; both of these methods suggest that the forward reaction has an associated barrier ($\Delta E_1^{\ddagger}$) of 43 kJ mol^{-1}, with the reverse reaction ($\Delta E_2^{\ddagger}$) requiring 24 kJ mol^{-1}. Zero-point energy correction (ZPE) serves to raise these barriers slightly, but does not change the qualitative features of the reaction profile.

Of considerable interest are the data provided by ROMP2 and DFT methods; the former method provides values for $\Delta E_1^{\ddagger}$ and $\Delta E_2^{\ddagger}$ about 10 kJ mol^{-1} higher than G3(MP2)-RAD, while ROBHandHLYP/6-311++G(d,p) provides estimates of these barriers that are up to 40 kJ mol^{-1} higher than G3(MP2)-RAD. These are interesting data because in previous work BHandHLYP methods were capable of reproducing energy barriers calculated using CCSD(T) methods.[27–29] It is important to note that DFT methods were able to reproduce the difference in $\Delta E_1^{\ddagger}$ and $\Delta E_2^{\ddagger}$ calculated using the higher correlated methods and, as such, are capable of providing qualitative information concerning reaction mechanisms and trends.

Unfortunately, CCSD(T), G3(MP2)-RAD and ROMP2 methods are not suitable for the remaining systems of interest in this study because of resource limitations. Despite this, and for the reasons provided above, we chose to continue this study using ROBHandHLYP on the understanding that the absolute values for the activation energies are likely to be overestimated, while providing useful qualitative data. Data at other (lower) levels of theory are provided in the ESI.‡

Effect of radical, tether and leaving group

We next turned our attention to aryl radical **8** that proved, not unexpectedly, to cyclize very efficiently (97%) in our previous experimental study because it contained the good *tert*-butyl leaving group on the higher heteroatom (Scheme 5). Gratifyingly, ROBHandHLYP/6-311++G(d,p) calculations indicate that this reaction is significantly exothermic (37 kJ mol^{-1}) with a barrier of 44.5 kJ mol^{-1}, significantly lower than that calculated for the benchmark example (Scheme 4) at the same level of theory. The transition structure **9** involved in this reaction is displayed in Fig. 2‡ and reveals key bond distances of 2.199 and 1.910 Å that are consistent with a significantly "earlier" transition structure than **7**.

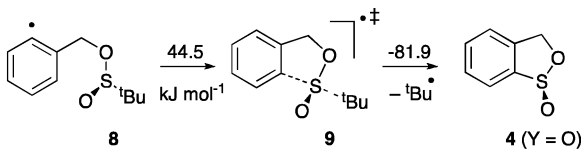

Scheme 5

When the *tert*-butyl group is replaced by phenyl, the potential energy surface now reveals the existence of a hypervalent intermediate **12** and an alternative reaction channel leading to biaryl products (Scheme 6). In the case of the sulfinate **10** (Y = O),‖ ROBHandHLYP/6-311++G(d,p) calculations predict that **12** (Y = O) is formed with a barrier ($\Delta E_1^{\ddagger}$) of 43.6 kJ mol^{-1},

‖ The optimised structures of radicals **10** and **16** are global minima on their respective potential energy surface as determined by conformational searching at the ROBHandHLYP/6-31G(d) level of theory.

Table 2 BHandHLYP/6-311++G(d,p) calculated activation energies ($\Delta E_n^{\ddagger}$) for the reactions of radicals **10** and **16** (Scheme 6)

Entry	Radical	$\Delta E_1^{\ddagger a}$	$\Delta E_1^{\ddagger a}$ + ZPE	$\Delta E_2^{\ddagger a}$	$\Delta E_2^{\ddagger a}$ + ZPE	$\Delta E_3^{\ddagger a}$	$\Delta E_3^{\ddagger a}$ + ZPE	$\Delta E_4^{\ddagger a}$	$\Delta E_4^{\ddagger a}$ + ZPE	$\Delta E_5^{\ddagger a}$	$\Delta E_5^{\ddagger a}$ + ZPE	$\Delta E_6^{\ddagger a}$	$\Delta E_6^{\ddagger a}$ + ZPE
1	**10** (Y = O)	46.3	45.2	7.1	4.5	7.8	4.3	29.9	33.1	51.8	50.6	115.8	109.2
2	**10** (Y = NH)	48.9	48.0	5.1	3.1	4.3	1.4	23.8	27.8	69.1	66.4	115.9	109.2
3	**10** (Y = NMe)	53.5	51.9	4.4	2.4	6.0	3.0	38.1	41.9	63.7	61.4	114.7	108.1
4	**16**	68.0	66.4	1.8	–0.2	9.5	6.2	28.6	31.5	60.3	58.2	110.1	103.7

[a] Energies in kJ mol^{-1}.

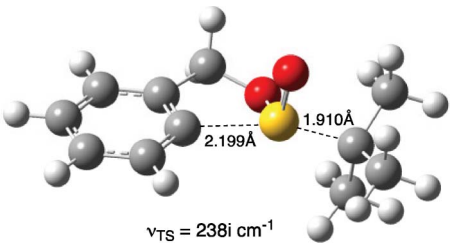

Fig. 2 ROBHandHLYP/6-311++G(d,p) optimised structure of transition state **9**.

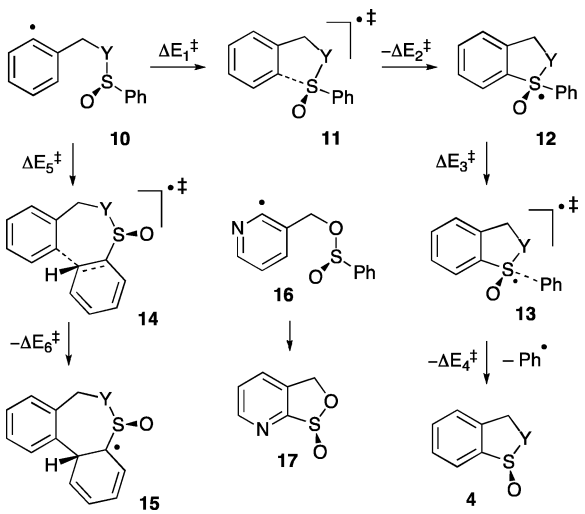

Scheme 6

a value that is very similar to that for the homolytic substitution process of **8** (Scheme 5). The intermediate **12** (Y = O) is predicted to lie in a shallow well, with barriers for dissociation ($\Delta E_2^{\ddagger}$, $\Delta E_3^{\ddagger}$) to the starting radical **10** and sultine **4** (Y = O) of 7.1 and 7.8 kJ mol^{-1}, respectively (Table 2, entry 1). In competition is the intramolecular homolytic addition of the radical centre in **10** to the aryl "leaving group" to form the adduct radical **15** *via* transition state **14**. The process is calculated to proceed with a barrier of 51.8 kJ mol^{-1} but is also exothermic by 64 kJ mol^{-1}, in contrast to the homolytic substitution channel which is calculated to be endothermic by about 14 kJ mol^{-1}.

Key features of structures **11–14**, calculated at the ROBHandHLYP/6-311++G(d,p) level of theory, are provided in Fig. 3.‡ It is interesting to note the arrangement of attacking and leaving groups in structures **11–13** (Y = O) that tend toward collinearity, with angles of 155–160° and the preferred *syn* arrangement of substituents (indicated by arrows in Fig. 3) in

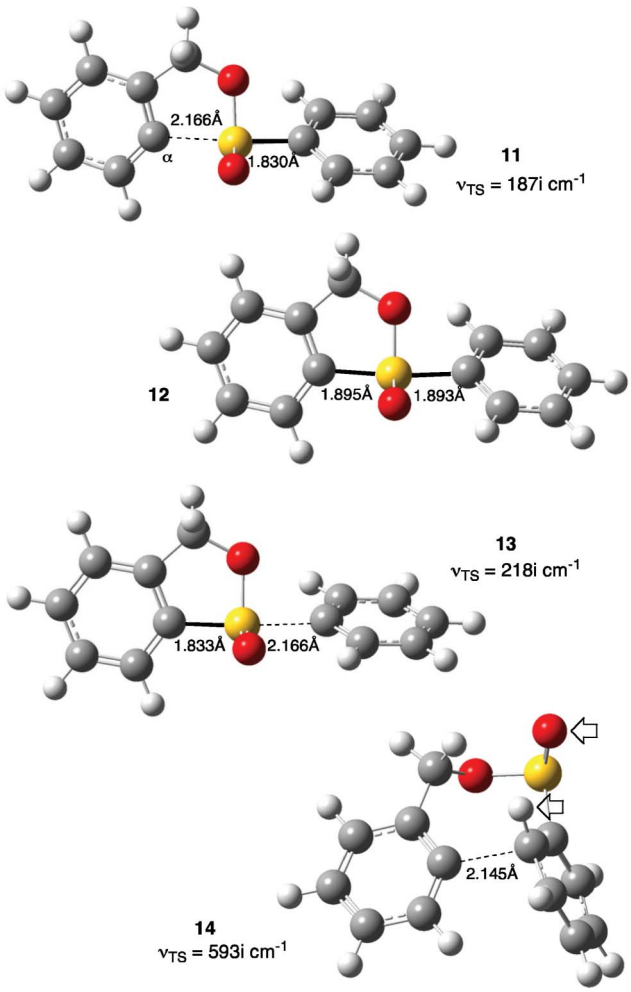

Fig. 3 ROBHandHLYP/6-311++G(d,p) optimised structures **11–14** (Y = O).

14; indeed the alternative *anti* arrangement was calculated to be higher in energy in each case and at each level of theory.

The data provided in Table 2 begin to provide an explanation for the products observed experimentally when the *p*-tolyl group is used in this chemistry (Scheme 3). Given that both barriers for the dissociation of **12** (Y = O) are similar and small, and given that the process leading to **4** is endothermic, it is reasonable to postulate that an equilibrium will be established between intermediate **12** (Y = O) and radical **10** (Y = O). This equilibrium will aid the formation of the biaryl adduct **15** as well as the formation of the sultine **4** whose formation is largely assured through favourable entropic factors.

It is interesting to note the effect of the tether (Y) in this chemistry. Replacement of O with NH (Table 2, entry 2) appears to have little effect on the homolytic substitution pathway, with a calculated barrier ($\Delta E_1^{\ddagger}$) of 48.9 kJ mol^{-1}, slightly higher than that calculated for the oxygen analogue (Y = O). Once again, the reaction is predicted to proceed through an intermediate **12** (Y = NH) that lies in a shallow well, before proceeding to the cyclic sulfinamide product **4** (Y = NH). In contrast, the energy barrier for the homolytic addition pathway ($\Delta E_5^{\ddagger}$) is calculated to be about 16 kJ mol^{-1} higher than that leading to **4**, suggesting that in the case of the sulfinamide-containg radical **10** (Y = NH), the reaction is more selective toward the homolytic substitution process. While cyclic sulfinamides such as **4** (Y = NH) were isolated from reaction mixtures, the small amounts of biaryl product **5** (Y = NH) that were observed experimentally could not be isolated due to their instability.[22]

The *N*-methylsulfinamide **10** (Y = NMe) is calculated to cyclise onto sulfur with an activation energy ($\Delta E_1^{\ddagger}$) of 53.5 kJ mol^{-1} (Table 2, entry 3), some 7 kJ mol^{-1} higher than its oxygen-tethered counterpart, and with a barrier ($\Delta E_5^{\ddagger}$) of 63.7 kJ mol^{-1} for intramolecular homolytic addition. The increase in $\Delta E_1^{\ddagger}$ over the other systems in this study (Table 2, entries 1, 2) may be partially responsible for the low yield of cyclised product **4** (Y = NMe) observed experimentally.[22]

Not surprisingly, the transition structures and intermediates **11–14** (Y = NH, NMe) are very similar to those in Fig. 3 and the interested reader is referred to Fig. S1 and S2 in the ESI.‡

In our previously-published experimental study,[22] we postulated that the low yield of cyclised sulfinamide **4** (Y = NMe) could be due to competing intramolecular hydrogen atom transfer (HAT) from the methyl substituent in radicals such as **10** (Y = NMe) (Scheme 7).

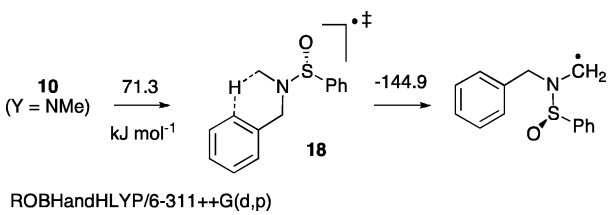

Scheme 7

As displayed in Scheme 7, ROBHandHLYP/6-311++G(d,p) calculations suggest that this HAT process, with an associated barrier of 71.3 kJ mol^{-1}, is unlikely to be competitive with homolytic substitution at sulfur, which is calculated to proceed with an energy barrier ($\Delta E_1^{\ddagger}$, Table 2, entry 3) about 18 kJ mol^{-1} lower.

The transition structure **18** for HAT is displayed in Fig. 4 and reveals transition state separations of 1.410 Å and 1.277 Å for the attacking and leaving vectors, respectively, with an attack angle of 143.8° (not shown).‡

Finally, we turned our attention to the chemistry of the pyridyl radical **16** leading to **17** (Scheme 6). Searching of the appropriate potential energy surface revealed similar features to the other surfaces explored as part of this work; the full reaction pathway is displayed in Scheme S1 in the ESI.‡ Radicals such as **16** have been shown to cyclise in poor yield[22] and we hoped that this computational study would shed some light on this observation.

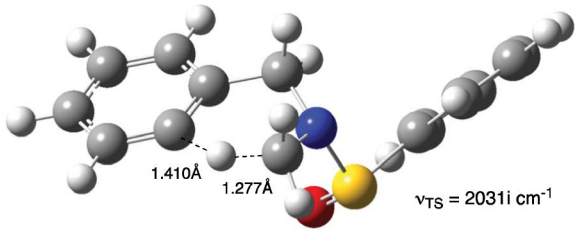

Fig. 4 ROBHandHLYP/6-311++G(d,p) optimized structure of HAT transition state **18**.

Consistent with experimental observation, cyclization of **16** to afford **17** is predicted to have an associated energy barrier ($\Delta E_1^{\ddagger}$, Table 2, entry 4) of 68.0 kJ mol^{-1}, almost 22 kJ mol^{-1} higher than the "parent" phenyl analogue **10** (Y = O). While an intermediate is calculated to be involved in this reaction, with zero-point energy correction, this species disappears, rendering the effective barrier ($\Delta E_1^{\ddagger}$ + $\Delta E_3^{\ddagger}$) 77.5 kJ mol^{-1}. Likewise, the homolytic addition reaction to form the analogous biaryl product is also calculated to have an increased barrier relative to the "parent" ($\Delta E_5^{\ddagger}$ = 60.3 kJ mol^{-1}); indeed, calculations predict that the homolytic addition pathway to form the biaryl adduct (**E**, Scheme S1) is preferred over the pathway leading to **17**. These results are consistent with the reduced reactivity of 2-pyridyl radicals compared to phenyl radicals, the former being resonance stabilised by the adjacent nitrogen atom.

While these calculated data provide a clear indication that **16** should react less efficiently than the other aryl radicals (**10**) in this study, it is instructive to examine the transition states **19** and **20** for the two competing reaction channels which are displayed in Fig. 5.‡ Both reaction pathways of **16** have "later" (in the direction of reaction, Scheme 4) transition states than the "parent", **10** (Y = O), consistent with the higher energy barriers discussed above. For intramolecular homolytic attack at sulfur, the transition state separation is calculated to be 2.096 Å (compared to 2.166 Å in **11** (Y = O)), while in the transition state for addition, the key

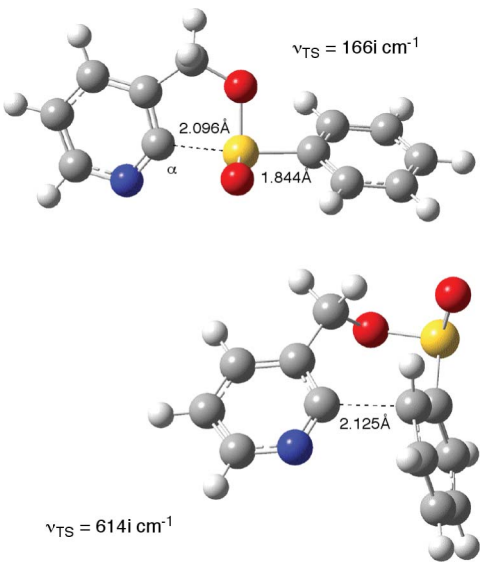

Fig. 5 ROBHandHLYP/6-311++G(d,p) optimised transition state structures for the intramolecular homolytic substitution (above) and homolytic addition (below) reactions of the pyridyl radical **16**.

separation is calculated to be 2.117 Å (compared to 2.145 Å in **14** (Y = O)).

The application of 2-pyridyl radicals in synthesis is uncommon and from the few reports that exist it appears that these radicals prefer to undergo *endo* cyclisation onto alkenes, which has been attributed to the "distorted geometry" of the 2-pyridyl radical and is caused by the overlap of the nitrogen lone pair with the radical centre (resonance stabilisation) as is observed for acyl radicals.[32–34] We have previously suggested that this distortion disfavours the homolytic substitution pathway and is, in part, responsible for the poor yields observed in our experiments.[22] This distortion is clearly evident in Fig. 5; ROBHandHLYP/6-311++G(d,p) calculations suggest that the key angle (α) is 125.9° in the transition state involving radical **16**, while the analogous angle in **11** (Y = O) is 131.3° (Fig. 3).

Conclusions

Ab initio and density functional theory (DFT) calculations predict that intramolecular homolytic substitution by alkyl radicals at the sulfur atom in sulfinates proceeds through a smooth transition state in which the attacking and leaving radicals adopt a near collinear arrangement. When forming a five-membered ring and when the leaving radical is methyl, G3(MP2)-RAD//ROBHandHLYP/6-311++G(d,p) calculations predict that this reaction proceeds with an activation energy ($\Delta E_1^{\ddagger}$) of 43.2 kJ mol^{-1}, up to 40 kJ mol^{-1} lower than that calculated using ROBHandHLYP methods. Despite this, ROBHandHLYP/6-311++G(d,p) is able to satisfactorily reproduce the qualitative features observed at the higher levels (G3, CCSD(T)) of theory and has been used to explore the chemistry of the larger systems in this study.

ROBHandHLYP/6-311++G(d,p) calculations suggest that the formation of five-membered rings through intramolecular homolytic substitution by aryl radicals at the sulfur atom in sulfinates and sulfinamides, with expulsion of phenyl radicals, proceeds with the involvement of hypervalent intermediates. These intermediates further dissociate to the observed products, with overall energy barriers of 45–68 kJ mol^{-1}, depending on the system of interest. In each case, homolytic addition to the phenyl group competes with substitution, with calculated barriers of 51–78 kJ mol^{-1}. This computational study complements and provides insight into previous experimental observations.

Acknowledgements

We thank the Australian Research Council through the Centres of Excellence Scheme for financial support. Support of the Australian Partnership for Advanced Computing National Facility and the School of Chemistry (University of Melbourne) High Performance Computing facility is also gratefully acknowledged.

References

1 C. H. Schiesser and L. M. Wild, *Tetrahedron*, 1996, **52**, 13265.
2 (*a*) J. C. Walton, *Acc. Chem. Res.*, 1998, **31**, 99; (*b*) D. Crich, *Helv. Chim. Acta*, 2006, **89**, 2167.
3 J. A. Kampmeier and T. R. Evans, *J. Am. Chem. Soc.*, 1966, **88**, 4096.
4 A. L. J. Beckwith and D. R. Boate, *J. Org. Chem.*, 1988, **53**, 4339.
5 A. L. J. Beckwith and S. A. M. Duggan, *J. Chem. Soc., Perkin Trans. 2*, 1994, 1509.
6 D. Crich and Q. Yao, *J. Org. Chem.*, 1996, **61**, 3566.
7 D. Crich and Q. Yao, *J. Am. Chem. Soc.*, 2004, **126**, 8232.
8 L. Benati, R. Leardini, M. Minozzi, D. Nanni, P. Spagnolo, S. Strazzari and G. Zanadri, *Org. Lett.*, 2002, **4**, 3079.
9 L. Benati, G. Calestani, R. Leardini, M. Minozzi, D. Nanni, P. Spagnolo and S. Strazzari, *Org. Lett.*, 2003, **5**, 1313.
10 (*a*) P. Carta, N. Puljic, C. Robert, A.-L. Dhimane, L. Fensterbank, E. Lacôte and M. Malacria, *Org. Lett.*, 2007, **9**, 1061; (*b*) P. Carta, N. Puljic, C. Robert, A. L. Dhimane, C. Ollivier, L. Fensterbank, E. Lacôte and M. Malacria, *Tetrahedron*, 2008, **64**, 11865.
11 C. H. Schiesser, *Chem. Commun.*, 2006, 4055 and references cited therein.
12 J. E. Lyons, C. H. Schiesser and K. Sutej, *J. Org. Chem.*, 1993, **58**, 1437.
13 M. A. Lucas, O. T. K. Nguyen, C. H. Schiesser and S.-L. Zheng, *Tetrahedron*, 2000, **56**, 3995.
14 N. Al-Maharik, L. Engman, J. Malmström and C. H. Schiesser, *J. Org. Chem.*, 2001, **66**, 6286.
15 R. L. Grange, J. Ziogas, A. J. North, J. A. Angus and C. H. Schiesser, *Bioorg. Med. Chem. Lett.*, 2008, **18**, 1241.
16 M. K. Staples, R. L. Grange, J. A. Angus, J. Ziogas, N. P. H. Tan, M. K. Taylor and C. H. Schiesser, *Org. Biomol. Chem.*, 2011, **9**, 473.
17 M. J. Laws and C. H. Schiesser, *Tetrahedron Lett.*, 1997, **38**, 8429.
18 I. Ryu, T. Okuda, K. Nagahara, N. Kambe, M. Komatsu and N. Sonoda, *J. Org. Chem.*, 1997, **62**, 7550.
19 M. K. Staples and C. H. Schiesser, *Chem. Commun.*, 2010, **46**, 565.
20 L. Engman, M. J. Laws, J. Malmström, C. H. Schiesser and L. M. Zugaro, *J. Org. Chem.*, 1999, **64**, 6764.
21 A. L. J. Beckwith and D. R. Boate, *J. Chem. Soc., Chem. Commun.*, 1986, 189.
22 (*a*) J. Coulomb, V. Certal, M.-H. Larraufie, C. Ollivier, J.-P. Corbet, G. Mignani, L. Fensterbank, E. Lacôte and M. Malacria, *Chem.–Eur. J.*, 2009, **15**, 10225; (*b*) J. Coulomb, V. Certal, L. Fensterbank, E. Lacôte and M. Malacria, *Angew. Chem., Int. Ed.*, 2006, **45**, 633.
23 **Gaussian 03:** M. J. Frisch, G. W. Trucks, H. B. Schlegel, G. E. Scuseria, M. A. Robb, J. R. Cheeseman, J. A. Montgomery, Jr., T. Vreven, K. N. Kudin, J. C. Burant, J. M. Millam, S. S. Iyengar, J. Tomasi, V. Barone, B. Mennucci, M. Cossi, G. Scalmani, N. Rega, G. A. Petersson, H. Nakatsuji, M. Hada, M. Ehara, K. Toyota, R. Fukuda, J. Hasegawa, M. Ishida, T. Nakajima, Y. Honda, O. Kitao, H. Nakai, M. Klene, X. Li, J. E. Knox, H. P. Hratchian, J. B. Cross, V. Bakken, C. Adamo, J. Jaramillo, R. Gomperts, R. E. Stratmann, O. Yazyev, A. J. Austin, R. Cammi, C. Pomelli, J. Ochterski, P. Y. Ayala, K. Morokuma, G. A. Voth, P. Salvador, J. J. Dannenberg, V. G. Zakrzewski, S. Dapprich, A. D. Daniels, M. C. Strain, O. Farkas, D. K. Malick, A. D. Rabuck, K. Raghavachari, J. B. Foresman, J. V. Ortiz, Q. Cui, A. G. Baboul, S. Clifford, J. Cioslowski, B. B. Stefanov, G. Liu, A. Liashenko, P. Piskorz, I. Komaromi, R. L. Martin, D. J. Fox, T. Keith, M. A. Al-Laham, C. Y. Peng, A. Nanayakkara, M. Challacombe, P. M. W. Gill, B. G. Johnson, W. Chen, M. W. Wong, C. Gonzalez and J. A. Pople, *GAUSSIAN 03 (Revision B.05)*, Gaussian, Inc., Wallingford, CT, 2004; **Gaussian 09**: M. J. Frisch, G. W. Trucks, H. B. Schlegel, G. E. Scuseria, M. A. Robb, J. R. Cheeseman, G. Scalmani, V. Barone, B. Mennucci, G. A. Petersson, H. Nakatsuji, M. Caricato, X. Li, H. P. Hratchian, A. F. Izmayl, J. Bloino, G. Zheng, J. L. Sonnenberg, M. Hada, M. Ehara, K. Toyota, R. Fukuda, J. Hasegawa, M. Ishida, T. Nakajima, Y. Honda, O. Kitao, H. Nakai, T. Vreven, J. A. Montgomery, Jr., J. E. Peralta, F. Ogliaro, M. Bearpark, J. J. Heyd, E. Brothers, K. N. Kudin, V. N. Staroverov, T. Keith, R. Kobayashi, J. Normand, K. Raghavachari, A. Rendell, J. C. Burant, S. S. Iyengar, J. Tomasi, M. Cossi, N. Rega, J. M. Millam, M. Klene, J. E. Knox, J. B. Cross, V. Bakken, C. Adamo, J. Jaramillo, R. Gomperts, R. E. Stratmann, O. Yazyev, A. J. Austin, R. Cammi, C. Pomelli, J. W. Ochterski, R. L. Martin, K. Morokuma, V. G. Zakrzewski, G. A. Voth, P. Salvador, J. J. Dannenberg, S. Dapprich, A. D. Daniels, O. Farkas, J. B. Foresman, J. V. Ortiz, J. Cioslowski and D. J. Fox, *GAUSSIAN 09 (Revision B.01)*, Gaussian, Inc., Wallingford, CT, 2010.
24 W. J. Hehre, L. Radom, P. v. R. Schleyer, P. A. Pople, *Ab Initio Molecular Orbital Theory*; Wiley, New York, 1986.
25 V. Tschinke and T. Ziegler, *Theor. Chim. Acta*, 1991, **81**, 65.
26 M. Mohr, H. Zipse, D. Marx and M. Parrinello, *J. Phys. Chem. A*, 1997, **101**, 8942.

27 S. M. Horvat and C. H. Schiesser, *New J. Chem.*, 2010, **34**, 1692.
28 S. H. Kyne, C. H. Schiesser and H. Matsubara, *J. Org. Chem.*, 2008, **73**, 427.
29 H. Matsubara, C. T. Falzon, I. Ryu and C. H. Schiesser, *Org. Biomol. Chem.*, 2006, **4**, 1920.
30 J. E. Lyons and C. H. Schiesser, *J. Chem. Soc., Perkin Trans. 2*, 1992, 1655.
31 C. H. Schiesser and L. M. Wild, *J. Org. Chem.*, 1999, **64**, 1131.
32 S. Maiti, B. Achari, R. Mukhopadhay and A. K. Banerjee, *J. Chem. Soc., Perkin Trans. 1*, 2002, 1769.
33 O. Kikuchi, Y. Hondo, Y. Yokoyama, K. Morihashi and M. Nakayama, *Bull. Chem. Soc. Jpn.*, 1991, **64**, 3448.
34 R. I. J. Amos, J. A. Smith, B. F. Yates and C. H. Schiesser, *Tetrahedron*, 2009, **65**, 7653.